International Journal of Minerals, Metallurgy and Materials
Volume 23, Number 3, March 2016, Page 358
DOI: 10.1007/s12613-016-1245-9

Enhanced photocatalytic activity of electrochemically synthesized aluminum oxide nanoparticles

Deepak Pathania[1)], *Rishu Katwal*[1)], *and Harpreet Kaur*[2)]

1) School of Chemistry, Shoolini University, Solan–173212 (H.P.), India
2) Department of Chemistry, Punjabi University, Patiala–147002 (Punjab), India
(Received: 7 August 2015; revised: 27 October 2015; accepted: 28 October 2015)

Abstract: In this study, aluminum oxide (Al_2O_3) nanoparticles (NPs) were synthesized via an electrochemical method. The effects of reaction parameters such as supporting electrolytes, solvent, current and electrolysis time on the shape and size of the resulting NPs were investigated. The Al_2O_3 NPs were characterized by Fourier transform infrared spectroscopy, X-ray diffraction, transmission electron microscopy, thermogravimetric analysis/differential thermal analysis, energy-dispersive X-ray analysis, and ultraviolet–visible spectroscopy. Moreover, the Al_2O_3 NPs were explored for photocatalytic degradation of malachite green (MG) dye under sunlight irradiation via two processes: adsorption followed by photocatalysis; coupled adsorption and photocatalysis. The coupled process exhibited a higher photodegradation efficiency (45%) compared to adsorption followed by photocatalysis (32%). The obtained kinetic data was well fitted using a pseudo-first-order model for MG degradation.

Keywords: aluminum oxide; nanoparticles; electrochemical preparation; photocatalysis

1. Introduction

Aluminum oxide (Al_2O_3) nanoparticles (NPs) have attracted significant attention because of their wide range of applications in different fields. Ceramics based on Al_2O_3 have been widely used by modern industry because of their unique properties such as high mechanical strength, high hardness, and good chemical stability. They have been used to create various catalytically active complexes for the oil industry and for cleaning industrial emissions [1]. Al_2O_3 is inert at room temperature and is insoluble in all ordinary chemical reagents. It exhibits excellent wear resistance and can be polished to a surface finish. Various allotropes of Al_2O_3 have been reported in the literature [1]; however, the α-Al_2O_3 phase is the most thermodynamically stable phase. Al_2O_3 NPs have been synthesized by many techniques such as ball milling, sol–gel, pyrolysis, sputtering, hydrothermal reactions, and laser ablation [2−10].

The electrochemical method of synthesizing NPs offers some important advantages such as it is a low-temperature growth method and cost effective. In addition, it provides controlled growth; thus, products can be obtained with preferred morphologies, structures, and orientations with specific advantages over other reported methods [11]. Because of such advantages of the electrochemical method, it has been explored for the synthesis of Al_2O_3 NPs.

The world is facing challenges associated with the purification of water and air resources. Organic pollutants such as benzidine, naphthalene, and other aromatic compounds have been introduced into the natural water system from textile, paper, dye intermediate, tannery, pharmaceutical, and kraft bleaching industries, among others. The main sources of severe pollution worldwide are the textile industry and its dye-containing wastewaters [12]. The dyeing process involves metals, salts, surfactants, sulfides, formaldehyde, and so on, which are used as additives to improve the adsorption of dyes onto fibers. The dye-containing effluents discharged into the water system are poisonous and carcinogenic [13].

The chemical name of malachite green (MG) is

Corresponding author: Deepak Pathania E-mail: dpathania74@gmail.com

4-{[4-(dimethylamino)phenyl] (phenyl)methylidene}-*N*,*N*-dimethylcyclohexa-2,5-dien-1-iminium chloride; its molecular formula and molar mass are $C_{23}H_{25}ClN_2$ and 364.91 g/mol, respectively. It has been extensively used as biocide in the global aquaculture industry and is highly effective against important protozoal and fungal infections [14–16]. MG dye has become one of the most debated and controversial compounds used in aquaculture because of risks it poses to consumers [15]. The use of this dye has been banned in several countries [17].

Thus, researchers have focused on the removal of MG and similar dyes from water systems. Various methods such as chemical oxidation, electrochemical treatment, liquid–liquid extraction, coagulation, photocatalysis, and adsorption have been investigated for the removal of dyes from water systems [18–23]. Among these methods, adsorption and photocatalysis have been demonstrated to be economical and efficient methods feasible for industrial-scale operation [24]. Substantial changes have been observed in the chemical, mechanical, physical, and optical properties of adsorbents when their particle size is reduced to the nanometer scale. The most prominent observed changes are increased surface area and altered structure of the pores, which increase materials' adsorption capacity [25].

Photocatalysis is a highly active research field because of its numerous potential applications. The photocatalytic detoxification of wastewater through the combination of heterogeneous catalysis with solar technologies has been reported [26]. Different photocatalytic materials such as ZnO, CuO, TiO_2, CdS, and Fe_2O_3 have been effectively used to degrade different dyes [27–30]. To the best of our knowledge, no study has reported the relationship between the reaction parameters used to prepare Al_2O_3 NPs and the resulting NPs' ability to photocatalytically degrade MG dyes.

In the present study, Al_2O_3 NPs were synthesized electrochemically. The effects of the electrolyte, solvent, current, and electrolysis time on the shape and size of the resulting NPs were investigated. The prepared Al_2O_3 NPs were subsequently characterized by X-ray diffraction (XRD), Fourier transform infrared spectroscopy (FTIR), and transmission electron microscopy (TEM). Adsorption followed by photocatalysis and coupled adsorption and photocatalytic processes were subsequently used for the remediation of MG dye from an aqueous system.

2. Experimental

2.1. Synthesis of Al_2O_3 NPs

The electrochemical deposition of Al_2O_3 NPs has been previously reported [11]. In a typical procedure, 1.25 mmol/L of supporting electrolyte (sodium hydroxide (SH), sodium carbonate (SC), and sodium nitrate (SN)) was dissolved in 200 mL of solvent (water, water:acetonitrile (water–ACN) (12:1), or water:methanol (12:1)). An aluminum plate (2 cm× 5 cm) and an inert platinum electrode (1 cm× 1 cm) were used as a sacrificial anode and cathode, respectively. Before electrochemical deposition, both electrodes were cleaned with hydrochloric acid and then with double-distilled water. The distance between the electrodes was fixed at 1 cm for all of the experiments. The electrolysis reaction was conducted in an undivided electrochemical cell for 2 h with vigorous stirring at room temperature. The electrolysis reaction was performed at different currents (20 mA, 50 mA, and 100 mA). After the electrolysis, the white precipitates were centrifuged, washed with ethanol, and finally washed with distilled water. The products were then dried at 60°C in a hot-air oven for 2 h. The materials obtained under different conditions were calcined at 900, 1100, and 1200°C for 1 h to study the effect of temperature on the size of the particles. The electrolytic cell is presented in Fig. 1.

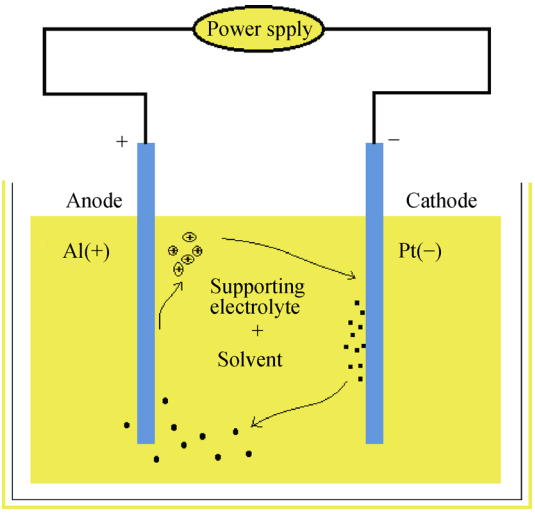

Fig. 1. Schematic of the electrochemical cell used to deposit Al_2O_3 NPs.

2.2. Photocatalytic degradation studies

The photocatalytic degradation of MG dye was performed using Al_2O_3 NPs under solar irritation. In a typical procedure, 100 mg of Al_2O_3 NPs was added to 1.5×10^{-5} mol/L solution of MG dye to form a suspension [23,31]. The adsorption and photocatalytic studies were performed using a Pyrex glass beaker and a magnetic stirrer for controlled agitation. During adsorption experiments, the suspension was maintained in darkness for adsorption and desorption of MG dye. After equilibrium was established, the

suspension was exposed to sunlight with intermittent agitation for photocatalysis. Prior to the photocatalysis studies, the suspension composed of dye and composite was stirred continuously. During the reaction, 5 mL of solution was withdrawn at different time intervals and centrifuged. The photocatalytic degradation of the MG dye was investigated at 620 nm. The degradation percentage of dye was calculated according to the formula

$$\text{Degradation}=\frac{C_e - C_t}{C_e}\times 100\% \quad (1)$$

where C_e and C_t are the concentrations of dye at equilibrium and at time t, respectively.

The rate of photodegradation of dye was fit using a pseudo-first-order kinetics model as follows [32–34]:

$$\ln\left(C_0 / C_t\right) = -k_{app}t \quad (2)$$

where C_0 is the concentration of dye before illumination, and k_{app} is the apparent rate constant.

2.3. Characterization

FTIR (Perkin-Elmer, Spectrum RX-IFTIR) spectra of Al_2O_3 NPs were recorded using the KBr disc method. The crystal structure of the Al_2O_3 NPs was determined by powder XRD on a diffractometer (PANalytical X'Pert) equipped with a Cu K_α radiation source (λ = 0.15418 nm) operated at 50 kV and 200 mA. TEM/energy-dispersive X-ray analysis (FEI Tecnai F20) were performed by dropping diluted solutions of Al_2O_3 NPs onto copper grids covered with a thin amorphous carbon film; the microscope was operated at an accelerating voltage of 200 kV.

3. Results and discussion

The electrochemical synthesis of Al_2O_3 NPs was influenced by numerous reaction parameters, including the nature of the electrolyte, electrode, solvent, temperature, dimensions of the cell, and the current. The effect of these reaction parameters on the synthesis of Al_2O_3 NPs is discussed in the following sections.

3.1. Effect of electrolyte

Electrochemical synthesis is a soft chemical technique; it was used in this work to prepare Al_2O_3 NPs. Electrochemical synthesis depends upon the nature of the supporting electrolyte. The supporting electrolyte can change the acid–base character of the solution, participate by attacking intermediate species, alter product distribution, stabilize the growth of particles in the solution, and increase the rate of reaction [35]. During the electrochemical process, the bulk aluminum at the anode is oxidized to aluminum ions, which migrate to the cathode, where reduction occurs in conjunction with the formation of adatoms [35]. We investigated the effect of different supporting electrolytes (SH, SN, and SC) while keeping the current, electrolysis time, and solvent system constant. We observed that the color of the electrolyte solution changed from colorless to a light-milky-white suspension over a period of a few minutes. This change was due to the transformation of aluminum into Al_2O_3 particles through a series of reactions: $Al \rightarrow Al^{3+} \rightarrow Al(OH)_2 \rightarrow Al_2O_3$. We further confirmed these results using XRD and TEM, as shown in Figs. 2–5. The measured product yield was higher in the presence of SC as the electrolyte than in the presence of SH or SN as the electrolyte.

Control of the morphology, size, and purity of Al_2O_3 NPs can be achieved by complete understanding of the reaction mechanism of electrodeposition. On the basis of our results, we deduced the following possible mechanisms for generating Al_2O_3 NPs in the presence of SH, SC, and SN electrolytes.

In the presence of NaOH electrolyte:

$Al \rightarrow Al^{3+} + 3e^-$ at anode;

$OH^- + 2H_2O + 2e^- \rightarrow 3OH^- + H_2$ at cathode;

$2Al^{3+} + 6OH^- \rightarrow \gamma\text{-}Al_2O_3 + 3H_2O$ in electrolyte solution.

In the presences of Na_2CO_3 electrolyte:

$Al \rightarrow Al^{3+} + 3e^-$ at anode;

$CO_3^{2-} + H_2O \rightarrow 2OH^- + CO_2$ at cathode;

$2Al^{3+} + 6OH^- \rightarrow \gamma\text{-}Al_2O_3 + 3H_2O$ in electrolyte solution.

In the presence of $NaNO_3$ electrolyte:

$Al \rightarrow Al^{3+} + 3e^-$ at anode;

$NO_3^- + H_2O + 2e^- \rightarrow 2OH^- + NO_2^-$ at cathode;

$2Al^{3+} + 6OH^- \rightarrow \gamma\text{-}Al_2O_3 + 3H_2O$ in electrolyte solution.

During calcination (in all cases):

$$\gamma\text{-}Al_2O_3 \xrightarrow{900^\circ C} \delta\text{-}Al_2O_3 \xrightarrow{1100^\circ C}$$
$$\theta\text{-}Al_2O_3 \xrightarrow{1200^\circ C} \alpha\text{-}Al_2O_3$$

When current was passed throught the electrolytic cell, OH^- and Al^{3+} ions were generated on the surface of the cathode and anode. Al^{3+} ions have been previously reported to react with OH^- ions to produce Al_2O_3 [36]. The nature of the electrolyte affects the shape and size of the NPs via the presence of different anions.

XRD analysis was used to confirm the purity and determine the phase of the NPs. Fig. 2 illustrates the XRD pattern of Al_2O_3 NPs synthesized in the presence of electrolytes SH, SC, and SN, with or without calcination. Broad and low-intensity diffraction peaks were observed at 2θ angles of approximately 39°, 45°, 60°, and 66°; these peaks are assigned

to γ-Al_2O_3 [37]. The samples obtained after calcination at 900°C and 1100°C contained mixed Al_2O_3 phases (θ-Al_2O_3 to α-Al_2O_3) (ICDD 29–0063, ICDD 48–0366). The γ-Al_2O_3 phase transforms to θ-Al_2O_3 at 700–800°C, and the metastable θ-Al_2O_3 phase transforms to the α-phase at approximately 1050°C. The phase transitions in Al_2O_3 are known to occur in the following sequence [38–40]:

γ-Al_2O_3 → δ-Al_2O_3 → θ-Al_2O_3 → α-Al_2O_3.

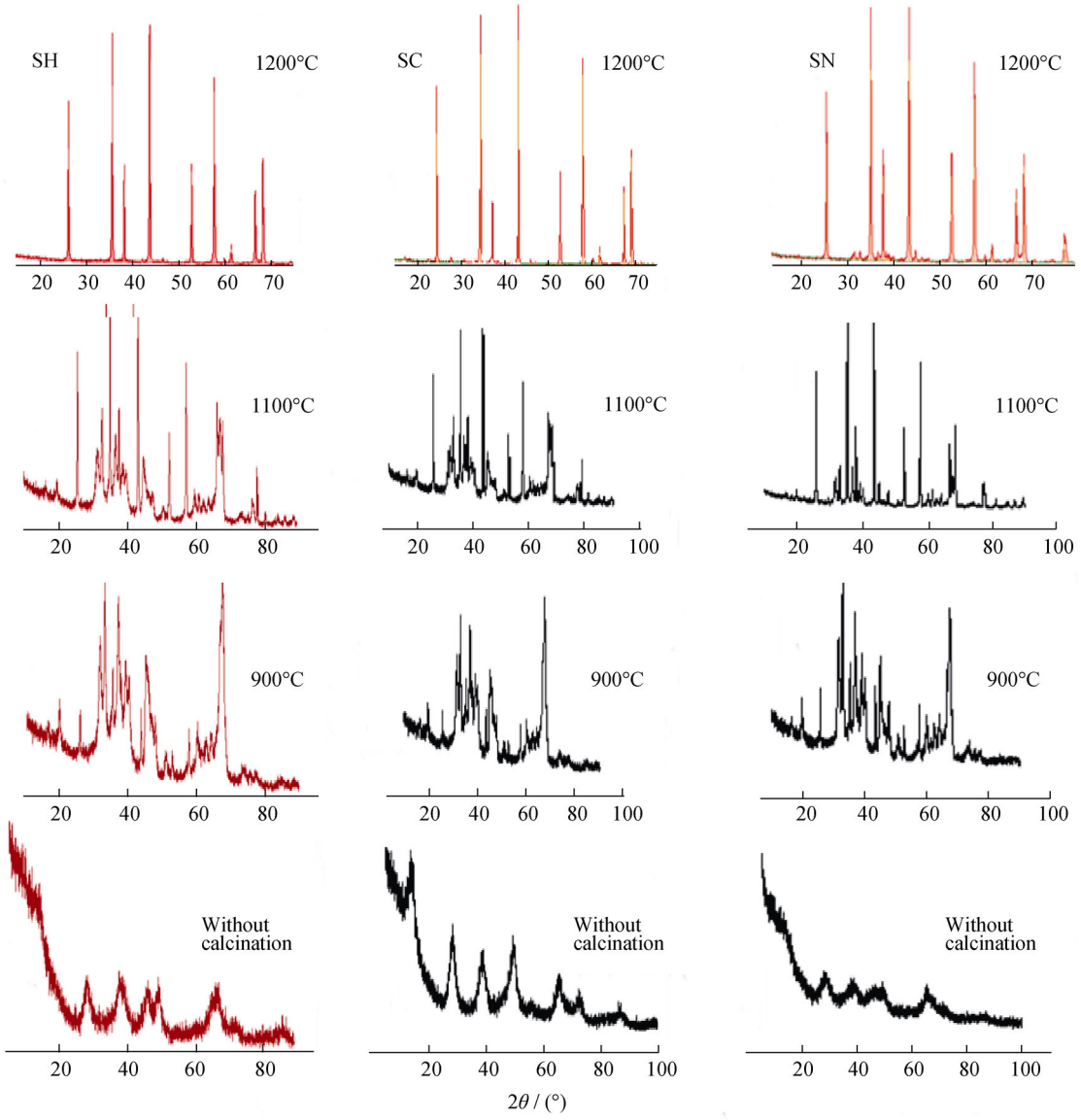

Fig. 2. XRD patterns of Al_2O_3 NPs prepared in the presence of sodium hydroxide (SH), sodium carbonate (SC), and sodium nitrate (SN) as the supporting electrolyte.

In the XRD pattern of Al_2O_3 NPs obtained after calcination at 1200°C, peaks corresponding to α-Al_2O_3 NPs (JCPDS No. 46-1212) were observed. A similar diffraction pattern was observed for the products obtained using all of the investigated electrolytes. The crystallinity of the Al_2O_3 NPs increased as the calcination temperature was increased from 900 to 1200°C. The peaks that appeared at 2θ values of 25.71°, 35.18°, 38.90°, 43.44°, 52.67°, 57.58°, 61.40°, 66.57°, 68.24°, and 77.01° correspond to the (012), (104), (110), (113), (024), (116), (018), (214), (300), and (119) lattice planes of Al_2O_3, respectively [41]. The size of the Al_2O_3 NPs was calculated from XRD data using the Debye–Scherrer equation. On the basis of the XRD results, the average crystallite sizes were calculated to be 33, 36, and 54 nm for NPs electrodeposited using SH, SC, and SN as electrolyte, respectively, and subsequently calcined at 1200°C.

Figs. 3–5 show the TEM micrographs of Al_2O_3 NPs prepared at a current of 100 mA using water–ACN as the solvent

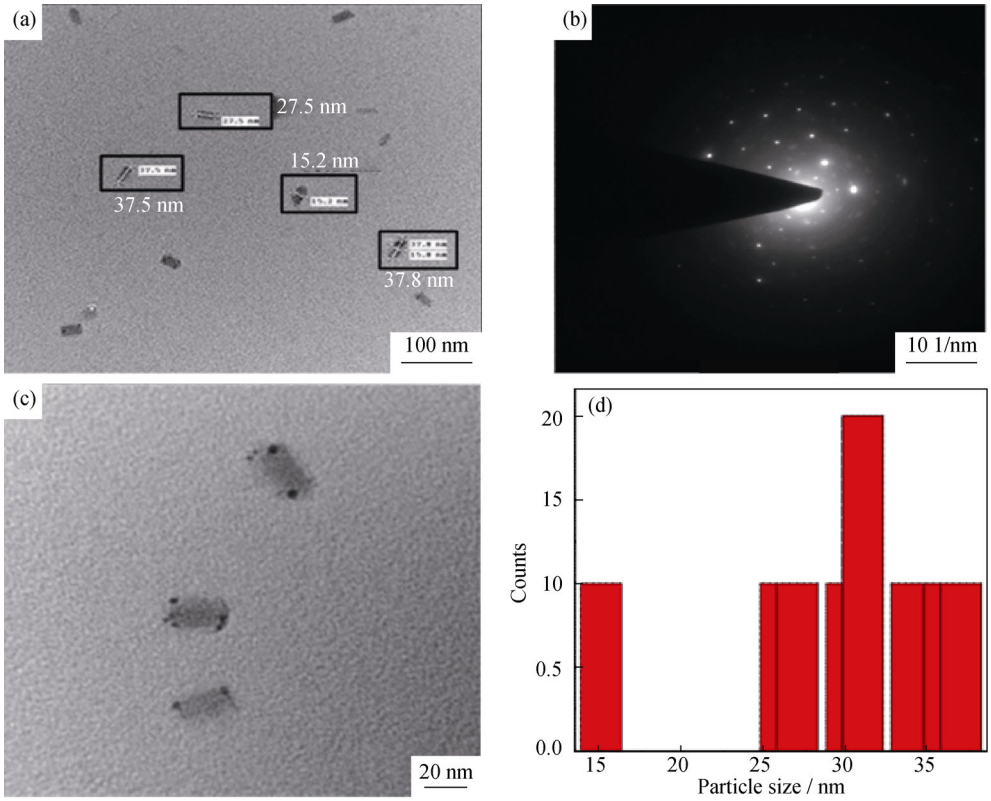

Fig. 3. (a) TEM micrographs, (b) SAAD pattern, (c) HRTEM image, and (d) particle size distribution of Al_2O_3 NPs synthesized in the presence of sodium hydroxide (SH) electrolyte.

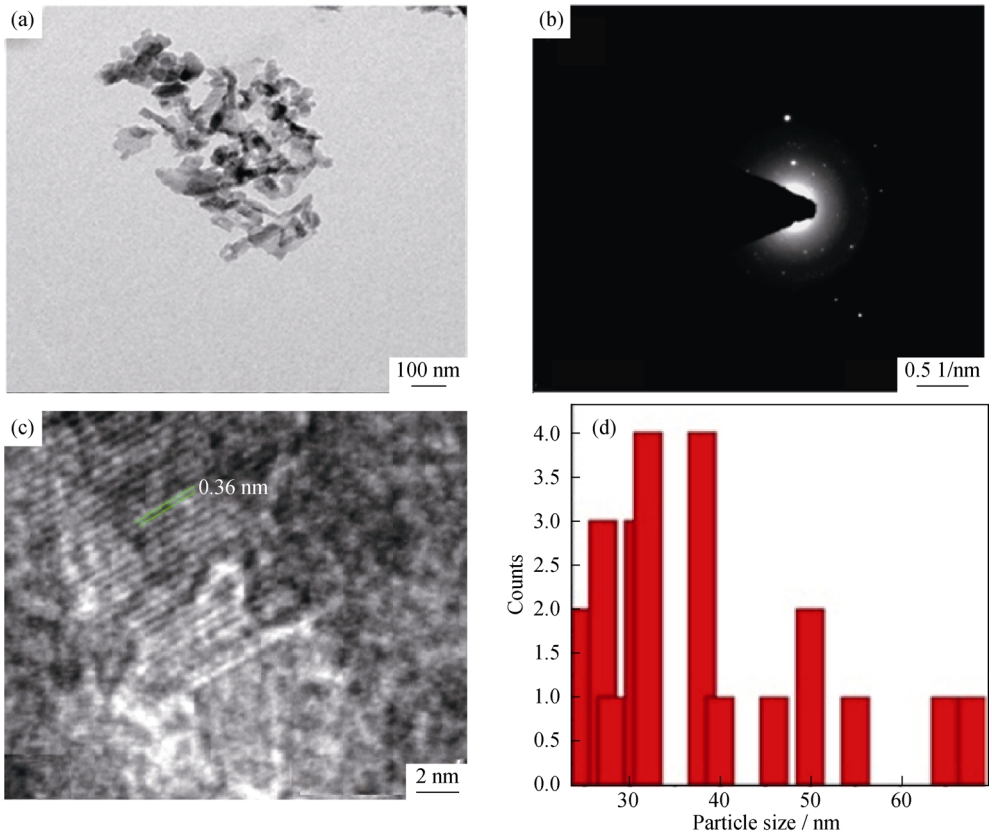

Fig. 4. (a) TEM micrographs, (b) SAAD pattern, (c) HRTEM image, and (d) particle size distribution of Al_2O_3 NPs synthesized in the presence of sodium carbonate (SC) electrolyte.

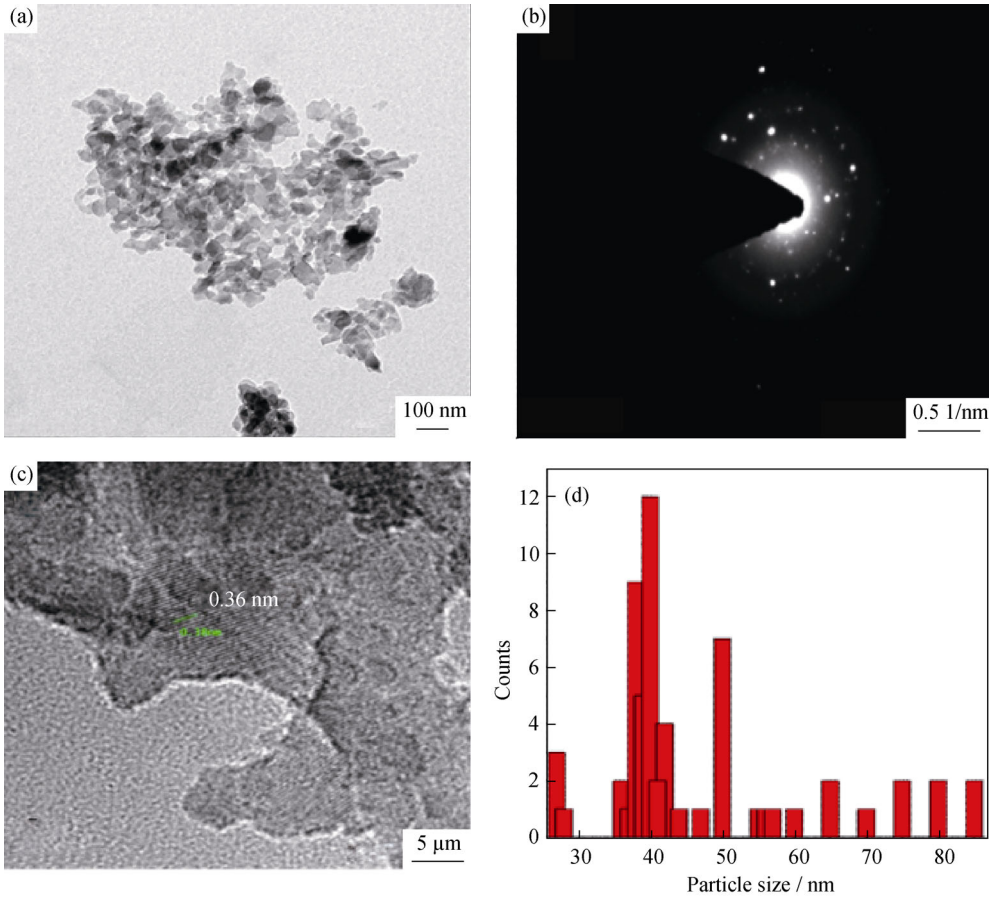

Fig. 5. (a) TEM micrograph, (b) SAAD pattern, (c) HRTEM image, and (d) particle size distribution of Al_2O_3 NPs synthesized in the presence of sodium nitrate (SN) electrolyte.

and various electrolytes (SH, SC, and SN). The TEM results indicate that nanobars with average grain sizes of 30 nm and 36 nm formed in the presence of SH and SC as the supporting electrolyte, respectively. By contrast, the product obtained when SN was used as the electrolyte consisted of spherical Al_2O_3 NPs with an average grain size of 43 nm. The selected-area electron diffraction (SAED) pattern revealed the crystalline and ordered orientations of the Al_2O_3 NPs (Fig. 3(c)). The lattice-plane spacing of 0.36 nm matches well with the (012) lattice plane of α-Al_2O_3 NPs, as inferred from Figs. 4(c) and 5(c). The high-resolution TEM (HRTEM) images are compatible with the XRD analysis results.

3.2. Effect of solvent

We studied the effects of different solvents such as water, water–methanol, and water–ACN at a deposition current of 100 mA and with SH as the supporting electrolyte. In an electrochemical reaction, the solvent contains dissolved ions, which are mobile and support current flow. The choice of solvent is an important factor in electrochemical synthesis. In our electrochemical system, a solvent with good solvation power was required to dissolve the reactants and products. A low viscosity was required to ensure rapid transport of reactants and products to and from the electrode, respectively [42]. A solvent with low reactivity was required to ensure compatibility with oxidizing and reducing electrodes and with reactive species created at the electrodes. Aprotic solvents provide reduction and oxidation limits beyond those achievable in aqueous solutions; thus, with aprotic solvents, a wider range of potential becomes available for electrochemical studies.

Acetonitrile is a polar aprotic solvent with high conductivity, good solvating power, high dielectric constant (ε = 37), and low toxicity; it has been used as a solvent for the fabrication of various metals and alloys [43]. We observed that the reaction solution turned from colorless to milky within a few minutes when water–ACN was used as the solvent as compared to when water and water–methanol were used as solvents. In addition, product yield was higher when water–ACN was used as the solvent compared to when water–methanol and water were used. The change in the shape and size of Al_2O_3 NPs prepared in different solvent media is shown in Fig. 6.

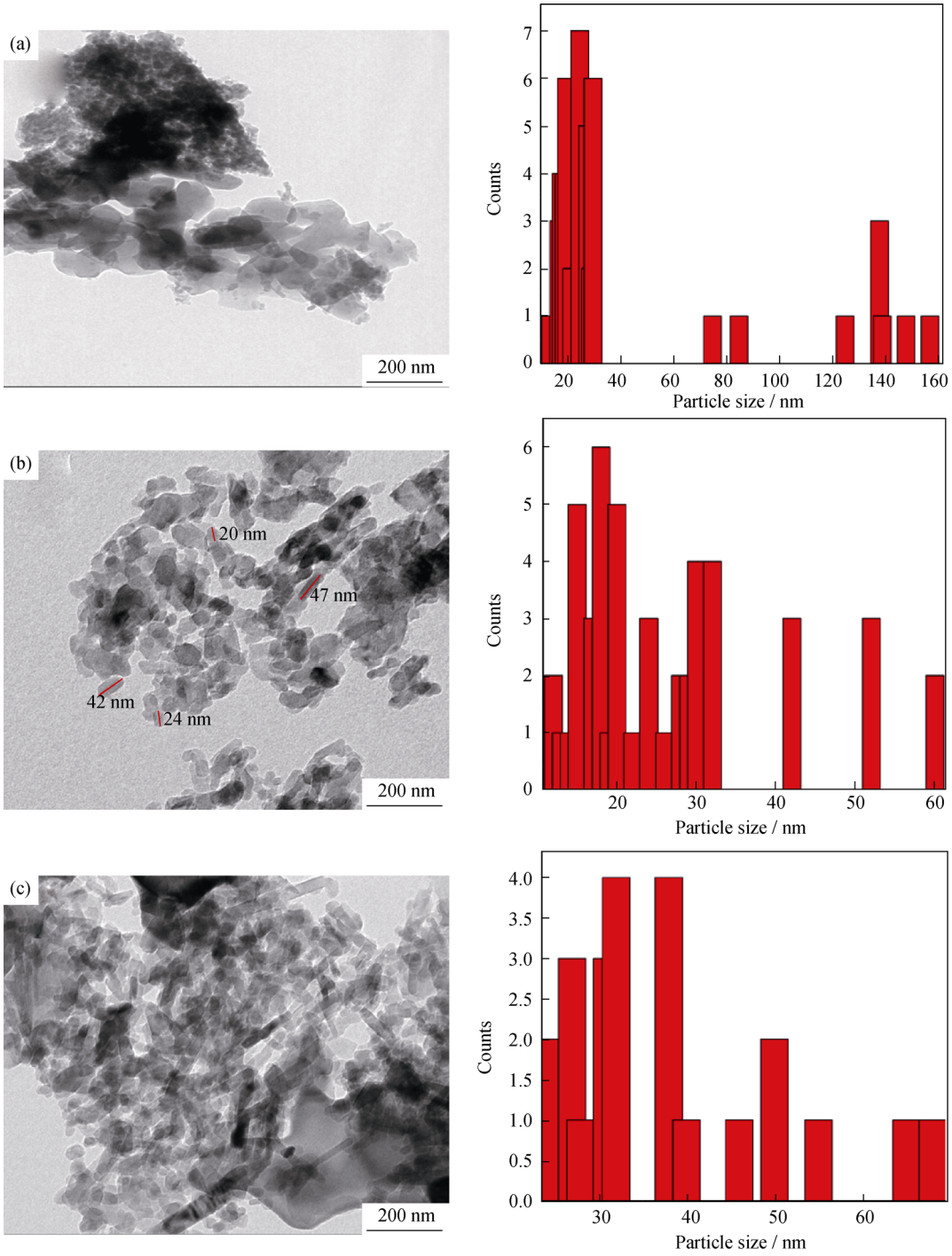

Fig. 6. TEM micrographs of Al_2O_3 NPs synthesized in the presence of (a) water solvent, (b) water–methanol solvent, and (c) water–acetonitrile solvent.

TEM micrographs revealed that the morphology of Al_2O_3 NPs was greatly influenced by the solvent. The Al_2O_3 NPs prepared in water as solvent contained two sets of agglomerates. The agglomerates of one set were small (average 20 nm in diameter), whereas those of the other set were large (average 140 nm), as shown in Fig. 6(a). TEM micrographs of the Al_2O_3 NPs clearly revealed the formation of smaller particles in water–methanol solvent (20–30 nm) compared to those formed in water–ACN solvent (30 nm). The results also showed that the morphology was changed by variation of the solvent.

3.3. Effect of current

The flow of current through the electrolyte as ions move

from anode to cathode depends upon the applied electrical field. To determine the effect of current, we conducted a series of reactions at currents of 20 mA and 50 mA in water–ACN (12:1) as the solvent and using SH (1.25 mmol/L) as the supporting electrolyte. During the electrolysis, changes in current visibly affected the color of the solution. At the highest investigated current of 100 mA, the color of the solution immediately turned milky white. Rapid generation of ions occurred at both the anode and cathode, which increased the rate of hydrogen evolution and also increased penetration and distribution of hydrogen bubbles through the bed of aluminum at the cathode surface [44]. At a current of 20 mA, ions were generated slowly and the color of the solution changed only slightly. We observed that the product yield increased with increasing current. The results clearly demonstrate that a high nucleation rate results in a smaller particles size. The change in particle size is attributable to the correlation between the current and particle size obtained from the free energy of formation of NPs [44].

The TEM results clearly show the effects of current on the particle size of Al_2O_3 NPs, as shown in Fig. 7. The particle size of the Al_2O_3 prepared at 20 mA was 50–60 nm; when the current was increased to 50 mA, the particle size decreased to 30–50 nm. The results show that the particle size was inversely proportional to the current.

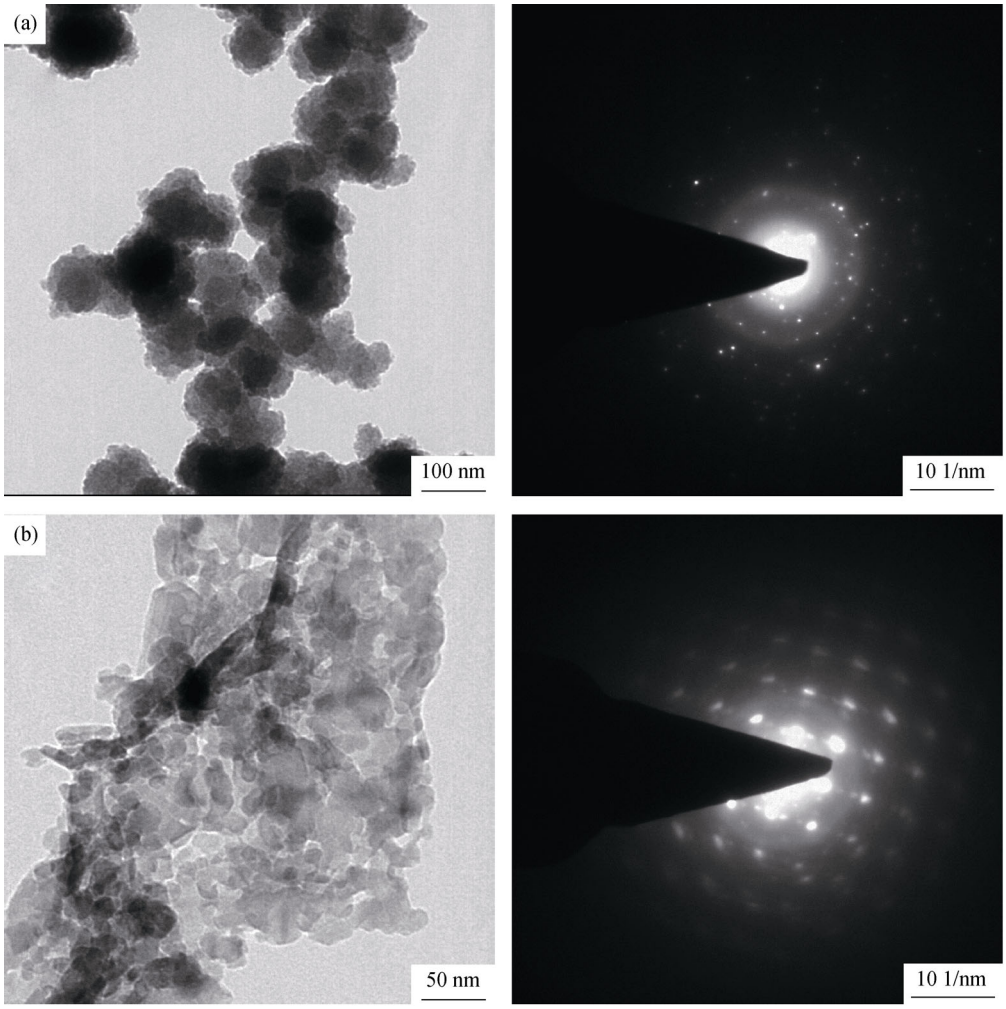

Fig. 7. TEM micrographs of Al_2O_3 NPs synthesized at currents of (a) 20 mA and (b) 50 mA.

3.4. Effect of electrolysis time

Al_2O_3 NPs were prepared in water–ACN (12:1) as solvent and SH (1.25 mmol/L) as the supporting electrolyte at a current of 100 mA for different electrolysis times (10, 30, and 60 min) at room temperature. We observed that, as the electrolysis time was increased from 10 to 60 min, the product yield was affected. At the longest electrolysis time of 60 min, more nuclei formed at the cathode surface compared to the number formed at electrolysis times of 30 min and 10 min. The size of the particles was also affected by the electrolysis time: as the electrolysis time was increased

from 10 min to 60 min, the nuclei size increased. Thus, electrolysis time was observed to be directly proportional to the particle size [45].

The influence of electrolysis time on the size of particles is shown in Figs. 8(a)–8(c). Incomplete formation of particles was observed after 10 min of electrolysis. Small-sized particles were formed at an electrolysis time of 30 min, and 25 nm particles were obtained at 60 min. Such increases in particle size were clearly observable in the TEM micrographs.

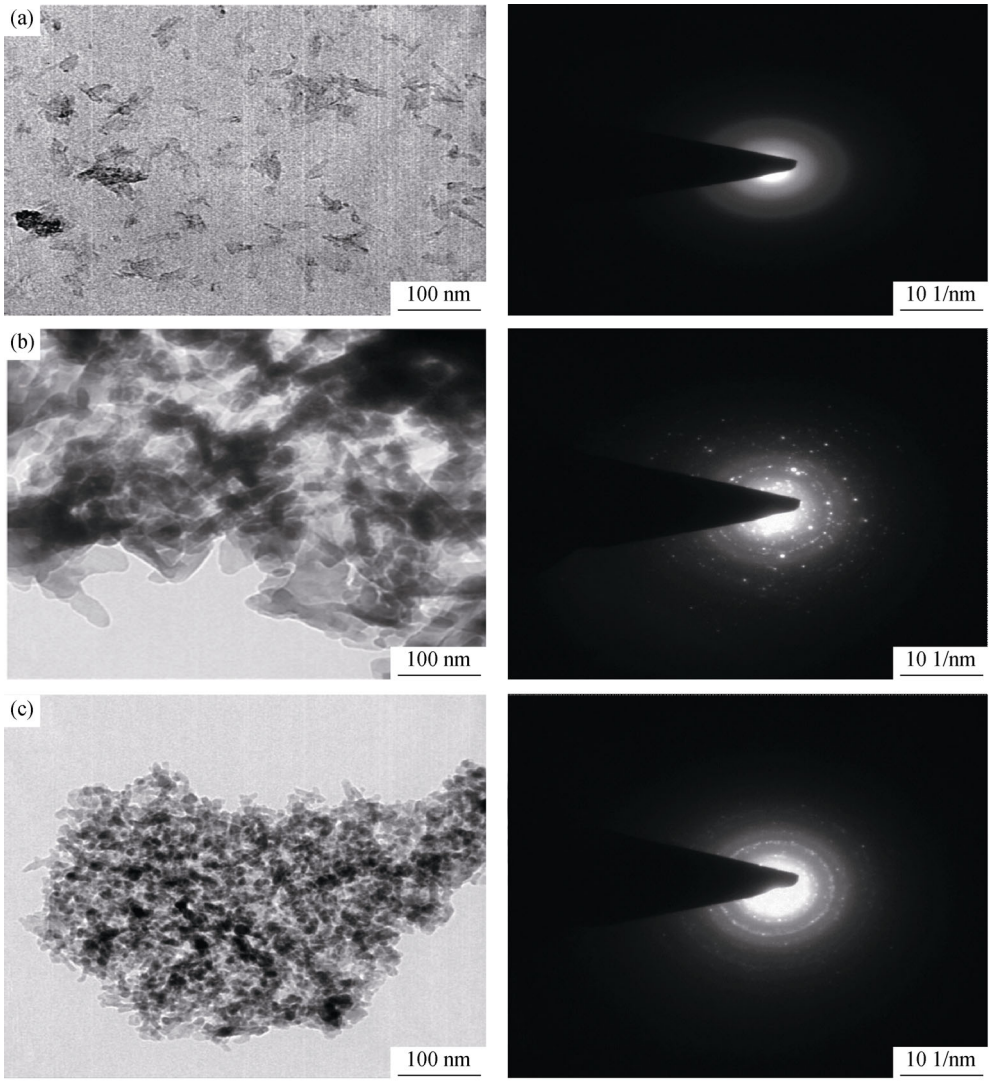

Fig. 8. TEM micrographs of Al_2O_3 NPs synthesized at different electrolysis times: (a) 10 min, (b) 30 min, and (c) 60 min.

The ultraviolet–visible (UV–Vis) spectrum of Al_2O_3 NPs calcined at 1200°C after being prepared using SH as the electrolyte, water–ACN as the solvent, and 100 mA of current is shown in Fig. 9. The UV–Vis absorption spectra of the Al_2O_3 NPs dispersed in distilled water show an absorption peak at approximately 210 nm. A strong absorption peak at 210 nm was clearly observed, which confirmed the presence of Al_2O_3 NPs in deionized water [46]. The band-gap energy of the synthesized Al_2O_3 NPs was calculated using the Tauc relation [47]:

$$\alpha hv = \beta(hv - E_g)^n \quad (3)$$

where α is the absorption coefficient (2.303 A/L), E_g is the optical band gap, hv is the photon energy, β is the band tailing parameter, and $n = 1/2$ for a direct band gap. The optical band gap was determined by extrapolating the straight portion of the curve of the plot of $(\alpha hv)^2$ vs. hv when $\alpha = 0$. The band gap was calculated from the Tauc plot to be 3.02 eV (Fig. 9(b)) [48].

The FTIR spectrum of the Al_2O_3 NPs is shown in Fig. 9(c). The band at 3467 cm^{-1} was due to O–H vibrations [49]. The peaks at 574 cm^{-1} and 826 cm^{-1} were attributed to Al–O bonds [50–51].

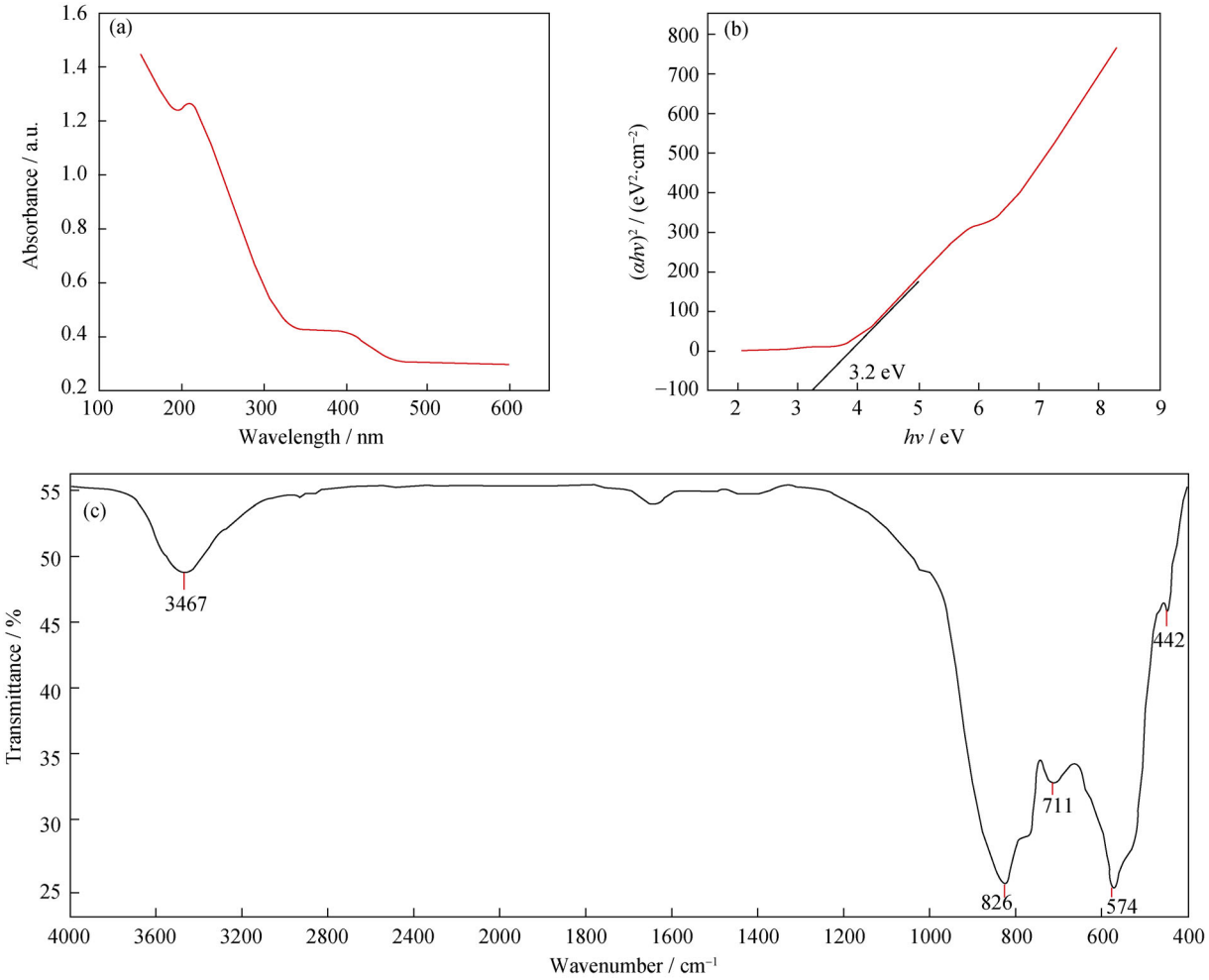

Fig. 9. (a) UV–Vis spectrum of Al_2O_3 NPs, (b) plot of $(\alpha h\nu)^2$ vs. $h\nu$ of Al_2O_3 NPs calcined at 1200°C, and (c) FTIR spectrum.

3.5. Thermal analysis

The thermogravimetric analysis (TGA) results for the prepared Al_2O_3 NPs are shown in Fig. 10. These results reveal that a total weight loss of 7.4% occurred between 100 and 600°C. The initial and final decomposition temperatures were 93 and 341°C, respectively. The observed weight loss may be due to the volatilization of surface-adsorbed water, which can exist stably to a certain temperature [52]. Differential thermal analysis studies of the Al_2O_3 NPs revealed a single exothermic peak at 58°C corresponding to the decomposition stage between 93 and 341°C.

3.6. Photocatalytic degradation of MG dye

The photocatalytic performance of the prepared Al_2O_3 NPs was studied under two processes: adsorption followed by photocatalysis and coupled adsorption and photocatalysis under sunlight irradiation, as shown in Fig. 11.

3.6.1. Adsorption followed by photocatalysis

Al_2O_3 NPs (SH electrolyte, water–ACN solvent, 100 mA current, calcined at 1200°C) were used to remove MG dye from aqueous media. Figs. 11(a) and 11(b) show a comparison of the degradation of dye in darkness and under solar-light irradiation at different time intervals. The characteristic absorption peak of MG at 620 nm was monitored as a function of the sunlight exposure time. The dye solution containing Al_2O_3 NPs was maintained in darkness to establish

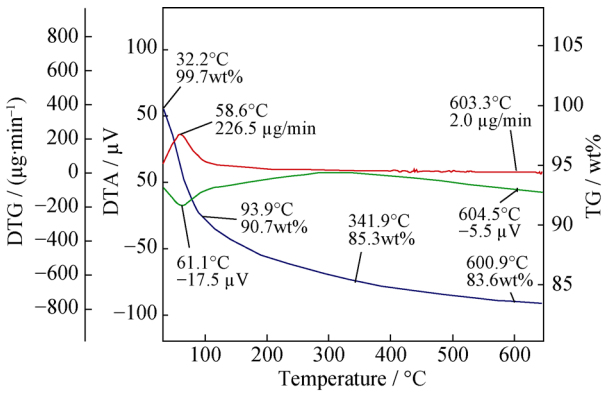

Fig. 10. TGA analysis of the prepared Al_2O_3 NPs.

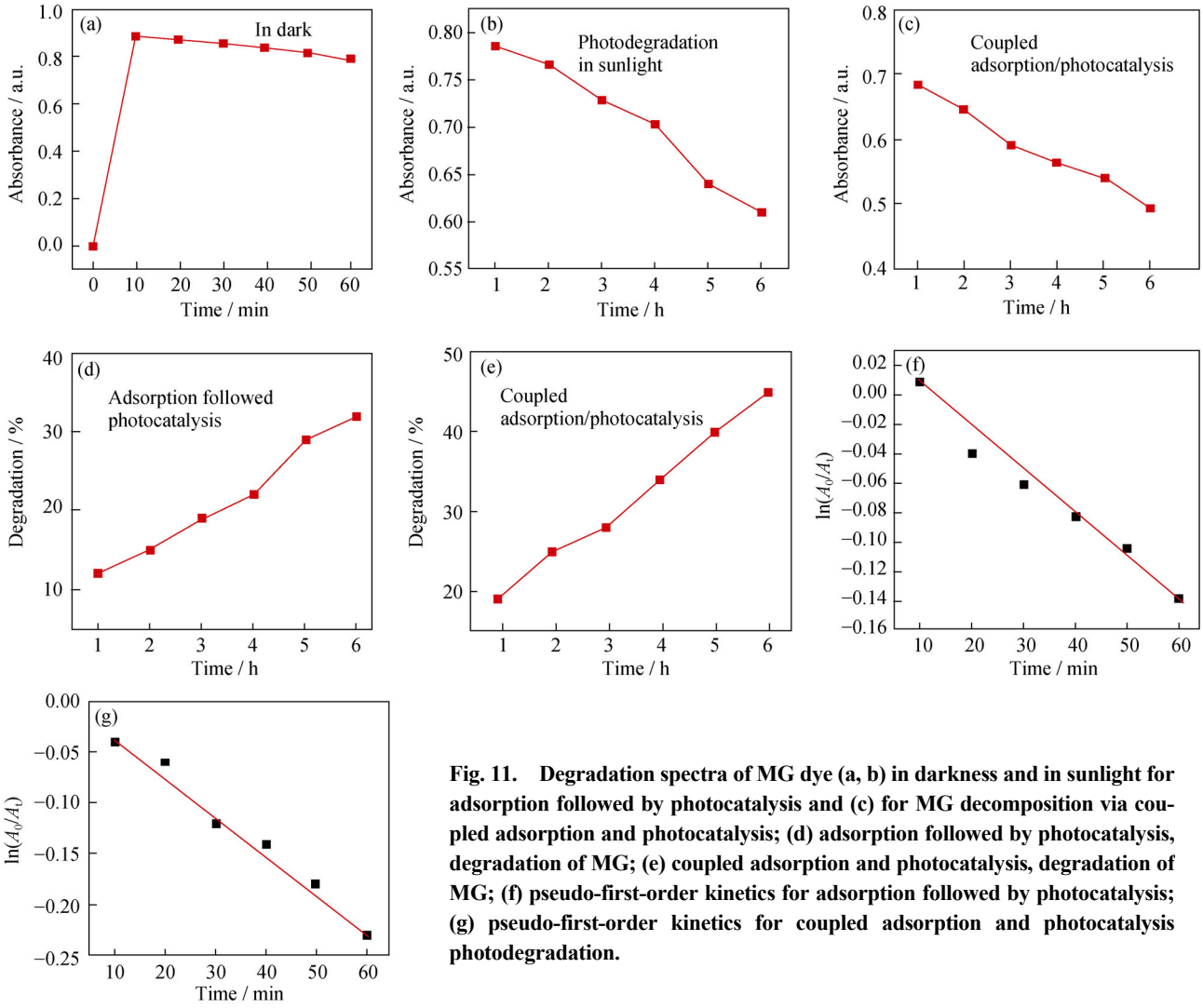

Fig. 11. Degradation spectra of MG dye (a, b) in darkness and in sunlight for adsorption followed by photocatalysis and (c) for MG decomposition via coupled adsorption and photocatalysis; (d) adsorption followed by photocatalysis, degradation of MG; (e) coupled adsorption and photocatalysis, degradation of MG; (f) pseudo-first-order kinetics for adsorption followed by photocatalysis; (g) pseudo-first-order kinetics for coupled adsorption and photocatalysis photodegradation.

an adsorption–desorption equilibrium. After 1 h of reaction in darkness, the suspension was exposed to solar light for further photodegradation. As evident in Fig. 11, the absorption peak at 620 nm slowly decreased in intensity with increasing irradiation time.

The dye suspension was first irradiated with solar light in the absence of a photocatalyst and was subsequently stirred with the Al_2O_3 NP photocatalyst. Only 12% of dye was adsorbed in 1 h under dark conditions, whereas 32% degradation was achieved by photocatalysis under solar irradiation for 5 h (Figs. 11(d) and 11(e)). During the adsorption equilibrium in darkness, the catalyst particles were highly covered by dye molecules, which might block light, resulting in lower degradation of MG. When the Al_2O_3 NPs were irradiated with light, electron–hole pairs were generated and reacted with water to produced hydroxyl and super oxide radicals, which break the conjugation of organic molecules. The plot of $\ln(A_0/A_t)$ vs. irradiation time in Fig. 11(f) shows a linear correlation (where A_e and A_t are the absorbance of dye at equilibrium and at time t, respectively). The pseudo-first-order rate constant k for dye photodegradation was calculated to be 0.02587, and the correction coefficient (R^2) was 0.97259.

3.6.2. Coupled adsorption and photocatalytic degradation

In the coupled adsorption and photocatalysis experiments, the effects of adsorption and photocatalysis on the degradation of MG were studied simultaneously. Fig. 11(c) shows the degradation of MG in the presence of Al_2O_3 NPs. Dye degradation of 45% was achieved in 6 h of dye illumination. The dye degradation follows pseudo-first-order kinetics, with a rate constant k of 0.00467 and a correction coefficient (R^2) of as shown in Fig. 11(g). This rate constant implies that the degradation in coupled adsorption and photocatalysis is higher than that in the case of adsorption followed by photocatalysis and clearly indicates that the extent of degradation under coupled adsorption and photocatalysis was

much higher than in the case of adsorption followed photocatalysis. Photocatalytic efficiency can be enhanced by adsorption onto the catalyst. As the MG adsorbs onto the Al_2O_3 NPs, simultaneous irradiation with sunlight leads to the generation of electron–hole (e^-–h^+) pairs in Al_2O_3. The electrons in the conduction band of Al_2O_3 interact with oxygen molecules adsorbed onto Al_2O_3 to form superoxide anion radicals (O^{-*}). The holes generated in the valence band of Al_2O_3 produce highly reactive hydroxyl radicals ($^*OH$) by reacting with surface hydroxyl groups. The photogenerated holes can lead to the production of OH radicals through the dissociation of water [31]. The highly reactive hydroxyl radicals ($^*OH$) and superoxide radicals (O^{-*}) react with MG adsorbed onto Al_2O_3 NPs and leads to the degradation of MG. The proposed mechanism for photodegradation of dye is as follows:

$Al_2O_3 + Dye \rightarrow Al_2O_3$–Dye,

$Al_2O_3(h^+) - Dye_{ads} + H_2O \rightarrow Al_2O_3(OH^*) - Dye_{ads} + H^+$,

$Al_2O_3(h^+) - Dye_{ads} + OH^- \rightarrow Al_2O_3(OH^*) - Dye_{ads}$,

$Al_2O_3(e^-_{CB}) - Dye_{ads} + O_2 \rightarrow Al_2O_3(O_2^{-*})$–Dye,

O_2^{-*} or OH^* + Al_2O_3 – Dye →

degradation product + Al_2O_3 for reuse ion.

where, subscripts ads and CB represent adsorption and conduction band, respectively.

4. Conclusions

Al_2O_3 NPs were successfully prepared by an electrochemical method. The Al_2O_3 NPs were characterized using different techniques such as FTIR, UV–Vis spectroscopy, XRD, and TEM. The results indicated that the electrolysis time and current strongly influenced the morphology and size of the resulting Al_2O_3 NPs. The electrolyte and solvent were observed to be the key factors influencing the shape and size of the NPs. The use of SH as the electrolyte resulted in smaller Al_2O_3 NPs compared to the NPs prepared using SC or SN as the electrolyte. Water–ACN was determined to be the best solvent for the electrochemical synthesis of Al_2O_3 NPs. TGA revealed that Al_2O_3 NPs prepared in water–ACN exhibited a greater thermal stability than Al_2O_3 NPs prepared in other solvents. The prepared Al_2O_3 NPs were used as a photocatalyst for the degradation of MG dye under two processes: adsorption followed by photocatalysis and coupled adsorption and photocatalysis under solar light for 6 h. The results clearly revealed that coupled adsorption and photocatalysis resulted in a greater degradation of the dye compared to adsorption followed by photocatalysis.

Acknowledgement

The authors are grateful to NIPER, Mohali, Punjab University, and IIT Roorkee for providing access to instrumentation.

References

[1] W.Q. Jiao, M.B. Yue, Y.M. Wang, and M.Y. He, Synthesis of morphology-controlled mesoporous transition aluminas derived from the decomposition of alumina hydrates, *Microporous Mesoporous Mater.*, 147(2012), No. 1, p. 167.

[2] C.B. Reid, J.S. Forrester, H.J. Goodshaw, E.H. Kisi, and G.J. Suaning, A study in the mechanical milling of alumina powder, *Ceram. Int.*, 34(2008), No. 6, p. 1551.

[3] F. Mirjalili, M. Hasmaliza, and L.C. Abdullah, Size-controlled synthesis of nano α-alumina particles through the sol–gel method, *Ceram. Int.*, 36(2010), No. 4, p. 1253.

[4] R. Kavitha and V. Jayaram, Deposition and characterization of alumina films produced by combustion flame pyrolysis, *Surf. Coat. Technol.*, 201(2006), No. 6, p. 2491.

[5] D.H. Trinh, M. Ottosson, M. Collin, I. Reineck, L. Hultman, and H. Högberg, Nanocomposite Al_2O_3–ZrO_2 thin films grown by reactive dual radio-frequency magnetron sputtering, *Thin Solid Films*, 516(2008), No. 15, p. 4977.

[6] L.H. Qu, C.Q. He, Y. Yang, Y.L. He, and Z.M. Liu, Hydrothermal synthesis of alumina nanotubes templated by anionic surfactant, *Mater. Lett.*, 59(2005), No. 29-30, p. 4034.

[7] K. Yatsui, T. Yukawa, C. Grigoriu, M. Hirai, and W. Jiang, Synthesis of ultrafine γ-Al_2O_3 powders by pulsed laser ablation, *J. Nanopart. Res.*, 2(2000), No. 1, p. 75.

[8] X.S. Peng, L.D. Zhang, G.W. Meng, X.F. Wang, Y.W. Wang, C.Z. Wang, and G.S. Wu, Photoluminescence and infrared properties of α-Al_2O_3 nanowires and nanobelts, *J. Phys. Chem. B*, 106(2002), No. 43, p. 11163.

[9] A. Rai, D. Lee, K. Park, and M.R. Zachariah, Importance of phase change of aluminum in oxidation of aluminum nanoparticles, *J. Phys. Chem. B*, 108(2004), No. 39, p. 14793.

[10] W.F. Li, X.L. Ma, W.S. Zhang, W. Zhang, Y. Li, and Z.D. Zhang, Synthesis and characterization of γ-Al_2O_3 nanorods, *Phys. Status Solidi A*, 203(2006), No. 2, p. 294.

[11] J.S. Banait, B. Singh, and H. Kaur, Electrochemical synthesis of zinc(II) phenoxides and their coordination compounds, *Portugaliae Electrochim. Acta*, 25(2007), No. 4, p. 435.

[12] D. Suteu, C. Zaharia, D. Bilba, R. Muresan, A. Popescu, and A. Muresan, Decolorization wastewaters from the textile industry: physical methods, chemical methods, *Ind. Textilă*, 60(2009), No. 5, p. 254.

[13] C. Zaharia, D. Suteu, A. Muresan, R. Muresan, and A. Popescu, Textile wastewater treatment by homogeneous oxidation with hydrogen peroxide, *Environ. Eng. Manage. J.*, 8(2009), No. 6, p. 1359.

[14] R.A. Schnick, The impetus to register new therapeutants for aquaculture, *Prog. Fish Cult.*, 50(1988), No. 4, p. 190.

[15] S. Srivastava, R. Sinha, and D. Roy, Toxicological effects of malachite green, *Aquat. Toxicol.*, 66(2004), No. 3, p. 319.
[16] S.J. Culp and F.A. Beland, Malachite green: a toxicological review, *Int. J. Toxicol.*, 15(1996), No. 3, p. 219.
[17] D.J. Alderman, Malachite green: a review. *J. Fish Dis.*, 8(1985), p. 298.
[18] E. Oguz and B. Keskinler, Comparison among O_3, PAC adsorption, O_3/HCO_3, O_3/H_2O_2 and O_3/PAC processes for the removal of Bomaplex Red CR-L dye from aqueous solution, *Dyes Pigm.*, 74(2007), No. 2, p. 329.
[19] R. Katwal, H. Kaur, G. Sharma, M. Naushad, and D. Pathania, Electrochemical synthesized copper oxide nanoparticles for enhanced photocatalytic and antimicrobial activity, *J. Ind. Eng. Chem.*, 31(2015), p. 173.
[20] T. Kim, C. Park, J. Yang, and S. Kim, Comparison of disperse and reactive dye removals by chemical coagulation and Fenton oxidation, *J. Hazard. Mater.*, 112(2004), No. 1-2, p. 95.
[21] D. Mohan, K.P. Singh, G. Singh, and K. Kumar, Removal of dyes from wastewater using flyash, a low-cost adsorbent, *Ind. Eng. Chem. Res.*, 41(2002), No. 15, p. 3688.
[22] S. Wang, Y. Booyjoo, A. Choueib, and Z.H. Zhu, Removal of dyes from aqueous solution using fly ash and red mud, *Water Res.*, 39(2005), No. 1, p. 129.
[23] V.K. Gupta, S. Agarwal, D. Pathania, N.C. Kothiyal, and G. Sharma, Use of pectin–thorium(IV) tungstomolybdate nanocomposite for photocatalytic degradation of methylene blue, *Carbohydr. Polym.*, 96(2013), No. 1, p. 277.
[24] P. Xu, G.M. Zeng, D.L. Huang, C. Lai, M.H. Zhao, Z. Wei, N.J. Li, C. Huang, and G.X. Xie, Adsorption of Pb(II) by iron oxide nanoparticles immobilized Phanerochaete chrysosporium: equilibrium, kinetic, thermodynamic and mechanisms analysis, *Chem. Eng. J.*, 203(2012), p. 423.
[25] M.N.V.R. Kumar, T.R. Sridhari, K.D. Bhavani, and P.K. Dutta, Trends in color removal from textile mill effluents, *Colourage*, 45(1998), No. 8, p. 25.
[26] D. Beydoun, R. Amal, G. Low, and S. McEvoy, Role of nanoparticles in photocatalysis, *J. Nanopart. Res.*, 1(1999), No. 4, p. 439.
[27] N. Serpone, D. Lawless, and E.Pelizzetti, Subnanosecond characteristics and photophysics of nanosized TiO_2 particulates from R_{part} = 10 A to 134 A: Meaning for heterogeneous Photocatalysis, *Fine Particles Sci. Technol.*, 12(1996), p. 657.
[28] T. Shiragami, S. Fukami, Y. Wada, and S. Yanagida, Semiconductor photocatalysis: effect of light intensity on nanoscale CdS-catalyzed photolysis of organic substrates, *J. Phys. Chem.,* 97(1993), No. 49, p. 12882.
[29] T. Murakata, R. Yamamoto, Y. Yoshida, M. Hinohara, T. Ogata, and S. Sato, Preparation of ultra fine TiO_2 particles dispersible in organic solvents and their photocatalytic properties, *J. Chem. Eng. Jpn.*, 31(1998), No. 1, p. 21.
[30] C. Kormann, D.W. Bahnemann, and M.R. Hoffmann, Environmental photochemistry: is iron oxide (hematite) an active photocatalyst? A comparative study: α-Fe_2O_3, ZnO, TiO_2, *J. Photochem. Photobiol. A*, 48(1989), No. 1, p. 161.
[31] V.K. Gupta, D. Pathania, N.C. Kothiyal, and G. Sharma, Polyaniline zirconium(IV) silicophosphate nanocomposite for remediation of methylene blue dye from waste water, *J. Mol. Liq.*, 190(2014), p. 139.
[32] S.A. Abo-Farha, Photocatalytic degradation of monoazo and diazo dyes in wastewater on nanometer-sized TiO_2, *J. Am. Sci.*, 6(2010), No. 11, p. 130.
[33] V.K. Gupta, D. Pathania, M. Asif, and G. Sharma, Liquid phase synthesis of pectin–cadmium sulfide nanocomposite and its photocatalytic and antibacterial activity, *J. Mol. Liq.*, 196(2014), p. 107.
[34] V.K. Gupta, T.A. Saleh, D. Pathania, B.S. Rathore, and G.A. Sharma, A cellulose acetate based nanocomposite for photocatalytic degradation of methylene blue dye under solar light, *Ionics*, 21(2015), No. 6, p. 1787.
[35] C.J. Huang, P.H. Chiu, Y.H. Wang, K.L. Chen, J.J. Linn, and C.F. Yang, Electrochemically controlling the size of gold nanoparticles, *J. Electrochem. Soc.*, 153(2006), No. 12, p. D193.
[36] T. Picard, G. Cathalifaud-Feuillade, M. Mazet, and C. Vandensteendam, Cathodic dissolution in the electrocoagulation process using aluminium electrodes, *J. Environ. Monit.*, 2(2000), No. 1, p. 77.
[37] B. Xu, J. Long, H. Tian, Y. Zhu, and X. Sun, Synthesis and characterization of mesoporous γ-alumina templated by saccharide molecules, *Catal. Today*, 147(2009), p. S46.
[38] H. Liu, G. Ning, Z. Gan, and Y. Lin, A simple procedure to prepare spherical α-alumina powders, *Mater. Res. Bull.*, 44(2009), No. 4, p. 785.
[39] R. Rogojan, E. Andronescu, C. Ghiţulica, and S.B. Vasile, Synthesis and characterization of alumina nano-powder obtained by sol-gel method, *UPB Sci. Bull. Ser. B.*, 73(2011), No. 2, p. 67.
[40] W.H. Gitzen, *Alumina as a Ceramic Material*, The American Ceramic Society, Columbus, 1970.
[41] J. Gangwara, K.K. Deya, K. Praveena, S.K. Tripathib, and A.K. Srivastavaa, Microstructure, phase formations and optical bands in nanostructured alumina, *Adv. Mater. Lett.*, 2(2011), No. 6, p. 402.
[42] C.G. Zoski, *Handbook of Electrochemistry*, Elsevier, 2007, p. 27.
[43] D.M. Seo, O. Borodin, D. Balogh, M. O'Connell, Q. Ly, S.D. Han, S. Passerini, and W.A. Henderson, Electrolyte solvation and ionic association: III. Acetonitrile–lithium salt mixtures–transport properties, *J. Electrochem. Soc.*, 160(2013), No. 8, p. A1061.
[44] A.H. Abbar, Electrolytic preparation of copper powder with particle size less than 63μm, *Al-Qadisiya J. Eng. Sci.*, 1(2008), No. 1, p. 32.
[45] H.S. Goh, R. Adnan, and M.A. Farrukh, ZnO nanoflake arrays prepared via anodization and their performance in the photodegradation of methyl orange, *Turk. J. Chem.*, 35(2011), No. 3, p. 375.
[46] V. Piriyawong, V. Thongpool, P. Asanithi, and P. Limsuwan,

Preparation and characterization of alumina nanoparticles in deionized water using laser ablation technique, *J. Nanomater.*, 2012(2012), art. No. 819403.

[47] F. Li, W. Bi, T. Kong, and Q.H. Qin, Optical and photocatalytic properties of novel CuS nanoplate-based architectutes synthesised by a solvothermal route, *Cryst. Res. Technol.*, 44(2009), No. 7, p. 729.

[48] V.S. Kortov, A.E. Ermakov, A.F. Zatsepin, and S.V. Nikiforov, Luminescence properties of nanostructured alumina ceramic, *Radiat. Meas.*, 43(2008), No. 2-6, p. 341.

[49] V. Srivastava, C.H. Weng, V.K. Singh, and Y.C. Sharma, Adsorption of nickel ions from aqueous solutions by nano alumina: kinetic, mass transfer, and equilibrium studies, *J. Chem. Eng. Data*, 56(2011), No. 4, p. 1414.

[50] A. Rabiezadeh, A.M. Hadian, and A. Ataie, Preparation of alumina/titanium diboride nano-composite powder by milling assisted sol–gel method, *Int. J. Refract. Met. Hard. Mater.*, 31(2012), p. 121.

[51] M.R. Karim, M.A. Rahman, M.A.J. Miah, H. Ahmad, M. Yanagisawa, and M. Ito, Synthesis of γ-alumina particles and surface characterization, *Appl. Sci.*, 4(2011), No. 5, p. 344.

[52] B. Sathyaseelan, I. Baskaran, and K. Sivakumar, Phase transition behavior of nanocrystalline Al_2O_3 powders, *Soft Nanosci. Lett.*, 3(2013). No. 4, p. 69.